ACS APPLIED MATERIALS & INTERFACES

Research Article

www.acsami.org

Cobalt-Releasing 1393 Bioactive Glass-Derived Scaffolds for Bone Tissue Engineering Applications

Alexander Hoppe,[†] Bojan Jokic,[‡] Djordje Janackovic,[‡] Tobias Fey,[§] Peter Greil,[§] Stefan Romeis,[∥] Jochen Schmidt,[∥] Wolfgang Peukert,[∥] Jonathan Lao,[⊥] Edouard Jallot,[⊥] and Aldo R. Boccaccini*[,†]

[†]Institute of Biomaterials, Department of Materials Science and Engineering, University of Erlangen-Nuremberg, Cauerstrasse 6, 91058 Erlangen, Germany

[‡]Faculty of Technology and Metallurgy, University of Belgrade, Karnegijava 4, 11000 Belgrade, Serbia

[§]Institute for Glass and Ceramic, Department of Materials Science and Engineering, University of Erlangen-Nuremberg, Martenstrasse 5, 91058 Erlangen, Germany

[∥]Institute of Particle Technology, Department of Chemical and Biological Engineering, University of Erlangen-Nuremberg, Cauerstrasse 4, 91058 Erlangen, Germany

[⊥]Laboratoire de Physique Corpusculaire, Clermont Université, Université Blaise Pascal, CNRS/IN2P3, BP 80026, 63171 Aubière Cedex, France

Supporting Information

ABSTRACT: Loading biomaterials with angiogenic therapeutics has emerged as a promising approach for developing superior biomaterials for engineering bone constructs. In this context, cobalt-releasing materials are of interest as Co is a known angiogenic agent. In this study, we report on cobalt-releasing three-dimensional (3D) scaffolds based on a silicate bioactive glass. Novel melt-derived "1393" glass (53 wt % SiO_2, 6 wt % Na_2O, 12 wt % K_2O, 5 wt % MgO, 20 wt % CaO, and 4 wt % P_2O_5) with CoO substituted for CaO was fabricated and was used to produce a 3D porous scaffold by the foam replica technique. Glass structural and thermal properties as well as scaffold macrostructure, compressive strength, acellular bioactivity, and Co release in simulated body fluid (SBF) were investigated. In particular, detailed insights into the physicochemical reactions occurring at the scaffold−fluid interface were derived from advanced micro-particle-induced X-ray emission/Rutherford backscattering spectrometry analysis. CoO is shown to act in a concentration-dependent manner as both a network former and a network modifier. At a concentration of 5 wt % CoO, the glass transition point (T_g) of the glass was reduced because of the replacement of stronger Si−O bonds with Co−O bonds in the glass network. Compressive strengths of >2 MPa were measured for Co-containing 1393-derived scaffolds, which are comparable to values of human spongy bone. SBF studies showed that all glass scaffolds form a calcium phosphate (CaP) layer, and for 1393-1Co and 1393-5Co, CaP layers with incorporated traces of Co were observed. The highest Co concentrations of ∼12 ppm were released in SBF after reaction for 21 days, which are known to be within therapeutic ranges reported for Co^{2+} ions.

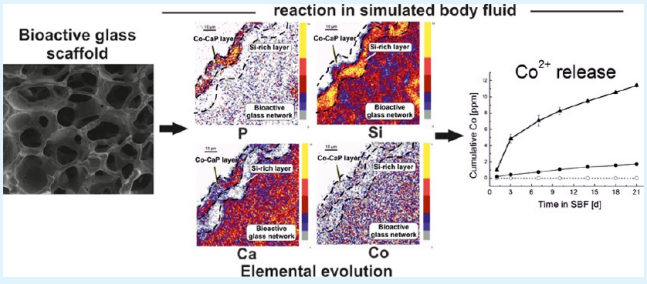

KEYWORDS: *cobalt, hypoxia, bioglass, bioactive, scaffold, bone tissue engineering, angiogenesis*

1. INTRODUCTION

Bioactive glasses (BGs), such as "45S5 Bioglass" (45 wt % SiO_2, 25 wt % CaO, 25 wt % Na_2O, and 6 wt % P_2O_5)[1] and "1393" (53 wt % SiO_2, 6 wt % Na_2O, 12 wt % K_2O, 5 wt % MgO, 20 wt % CaO, and 4 wt % P_2O_5) compositions,[2] have been widely used for bone tissue engineering applications. BGs allow strong bonding to hard as well as soft tissue and have been shown to promote osteogenesis via the activation of several relevant genes.[3] Bioactive glass-derived three-dimensional (3D) scaffolds have been extensively researched in tissue engineering approaches for restoring damaged tissue.[4] Hereby, a porous 3D network is seeded with cells that are stimulated toward proliferation and differentiation, resulting in the formation of bone tissue *in vitro*. However, after implantation *in vivo*, the new bone tissue needs a functioning blood supply, making neovascularization of bone constructs a critical issue.[5] Since it has become clear that highly vascularized tissue is essential for successful clinical application of engineered bone constructs,[5,6] research efforts have been focusing on enhancing the angiogenic potential of biomaterials by incorporating inorganic therapeutics into a carrier matrix.[7,8]

Received: November 28, 2013
Accepted: January 29, 2014
Published: January 29, 2014

BGs have been proposed as carrier platforms containing therapeutic ions that are released into the physiological medium upon degradation of the BG-derived scaffold.[9] A variety of inorganic ionic species have been suggested for use in regenerative medicine because of their stimulating effects on angiogenesis, osteogenesis, wound healing, and antibacterial potential.[8−10] Inorganic species such as metal ions, e.g., Cu^{2+}, Sr^{2+}, and Co^{2+}, are being considered as a possible alternative to growth factors and genetic approaches in tissue engineering because of their easy processing, stability at high temperatures, and tunable release kinetics.[11] A wide range of applications of such therapeutic ions integrated in an inorganic carrier matrix have been proposed, including Cu-containing 45S5 bioactive silicate glasses[12] and phosphate glasses[13] as well as calcium phosphates[14] and BG/alginate composites.[15] Controllable ion release kinetics is essential for clinical applications of such constructs to be able to avoid overly high levels of metallic ions exceeding their therapeutic limits from being released.[8,9]

Hypoxia induces pro-regenerative cellular processes by activating hypoxia inducible factor 1 (HIF-1). The HIF-1 pathways, in turn, accelerate bone regeneration[16] and are important for the development of angiogenesis, stem cell differentiation, and fracture repair.[17,18] Co is known to induce hypoxia conditions and in doing so to stabilize HIF-1.[19,20] Hence, Co-releasing bioactive glass has been proposed to be a hypoxia-mimicking material to be used for artificial stabilization of HIF-1, which is known to activate angiogenesis-related genes. Potential beneficial effects of Co^{2+} ions were further tested *in vitro* and *in vivo*. For instance, cobalt was shown to promote angiogenesis via activation of HIF-1 in a rat remnant kidney *in vivo* model when Co was applied by subcutaneous injections.[21] Also, in a rat bladder *in vivo* model, Co was shown to enhance hypoxia response, cell growth, and angiogenesis as evidenced by the stimulated expression of HIF-1α and vascular endothelial growth factor (VEGF).[22]

In addition, melt-derived Co-releasing glasses have been reported and proposed for use as hypoxia-mimicking biomaterials with controlled release of Co.[18] Sol−gel Co-containing bioactive glasses have been developed. Wu et al. used sol−gel-derived BG-derived scaffolds fabricated by the foam replica technique as a Co-releasing platform.[23] However, to the best of our knowledge, no Co-containing 1393 bioactive glass has been investigated so far. Moreover, no Co-containing highly porous scaffold with appropriate mechanical strength has been reported. Hence, the goal of this study was to fabricate Co-releasing mechanically robust 3D scaffolds based on 1393 bioactive glass suitable for applications in regenerative medicine. The influence of Co on the glass structure was investigated as it is known that glass chemistry strongly influences the reactivity of the bioactive glass indicated by the dissolution rate, dissolution pH, and release kinetics of the ions.[24]

Because degradation, ion release kinetics, and mineralization are factors known to dictate cell behavior and (bone) tissue formation, we investigated the *in vitro* reactivity of the scaffolds in simulated body fluid (SBF). Co release kinetics, degradation behavior, and the apatite forming ability of the 1393 scaffolds were observed.

Analysis of the elements present at the scaffold−SBF solution interface was conducted by the micro-PIXE-RBS (particle-induced X-ray emission/Rutherford backscattering spectrometry) technique, which has not yet been performed on 1393 bioactive glass scaffolds. These observations provide detailed insight into the physicochemical reaction occurring during the mineralization process and information about the chemical composition of the calcium phosphate layers formed at the surface of the scaffolds.

2. EXPERIMENTAL SECTION

2.1. Glass Fabrication. Co-containing bioactive glasses based on the 1393 composition were fabricated using silicic acid (pure, anhydrous) (Riedel de Haën), sodium carbonate (Riedel de Haën), potassium carbonate (Riedel de Haën), sodium dihydrogenphosphate (Riedel de Haën), magnesium carbonate (Lachner), calcium carbonate (Lachner), and cobalt nitrate (Carlo Erba) calculated to the glass composition (Table 1). All chemicals were p.a. grade. Melting was performed in a platinum crucible at 1400 °C for 2 h, and samples were rapidly cooled when the reactions were quenched in water. Fritted glass was then premilled in a jaw crasher (BB51, Retsch) and milled in a planetary mill (PM100, Retsch) using a ZrO_2 jar (Retsch) and ZrO_2 milling balls (Ø 5 mm, Retsch) to a final particle size ($d_{50,0}$) of ∼6 μm.

Table 1. 1393-Derived Glass Compositions (wt %) with Varying Amounts of CoO

	SiO_2	Na_2O	K_2O	P_2O_5	MgO	CaO	CoO
1393	53	6	12	4	5	20	–
1393-1Co	53	6	12	4	5	19	1
1393-5Co	53	6	12	4	5	15	5

2.2. Scaffold Fabrication. 3D scaffolds were produced using the foam replica technique as described previously.[25] Briefly, polyurethane foam (45 ppi, Recticel) was immersed in an aqueous slurry containing 60 wt % BG particles and 1.1 wt % polyvinyl alcohol (PVA) (Sigma) as a binder. The green bodies were dried at 60 °C for 24 h and subsequently sintered at 685, 680, and 670 °C for 1393, 1393-1Co, and 1393-5Co, respectively. For the mechanical tests, a second coating of the as-sintered scaffolds was performed. For this, the scaffolds were dip-coated with the BG slurry, and the excess slurry was removed by centrifugation. Afterward, the samples were sintered using the same heat treatment regime that was used for the first densification process.

2.3. Mechanical Testing. The compressive strength of the scaffolds (5 mm × 5 mm × 5 mm) was measured using a tensile testing machine (Z050, Zwick Roell). The testing speed was 10 mm/min. To ensure homogeneous loading of the scaffolds, a polymeric rubber interlayer was placed between the sample and the steel plates. Ten samples were measured per scaffold series, and the standard deviation was calculated. The sample size and deformation rate were chosen to prevent shear stress and delamination of the samples.

2.4. *In Vitro* Reactivity and Degradation in SBF. Scaffolds (5 mm × 5 mm × 5 mm) were immersed in a 50 mL SBF solution and kept in a shaking incubator (KS 4000i control, IKA) at 37 °C and 120 rpm. The SBF was prepared following the protocol defined by Kokubo et al.[26] The sample/liquid volume ratio used was chosen so that it was in agreement with previous investigations.[25] The samples were immersed in SBF for 21 days whereby the SBF solution was exchanged every 3 days and the ion concentration in the supernatant was analyzed by ICP-OES measurements.

2.5. Characterization Methods. *2.5.1. Scanning Electron Microscopy−Energy-Dispersive Spectroscopy (SEM−EDS).* For SEM analyses, the scaffolds were fixed on a sample holder with a dry conductive adhesive (Leit-C, Fluka Analytical). Before being imaged, the scaffolds were sputtered with gold. Images were taken with a FEI-Quanta 200 scanning electron microscope at an operation voltage of 20 kV. The thickness of reactive layers formed during immersion in SBF was estimated using ImageJ. Three points were measured on the sample, and the mean value was derived.

2.5.2. Porosity. The porosity P was calculated according to

$$P = 1 - \frac{\rho_{\text{foam}}}{\rho_{\text{solid}}}$$

with the density of the foam ρ_{foam} (calculated from the weight and volume) and the density of the solid 1393 glass ρ_{solid} (2.46 g/cm^3) (measured with Archimedes principle on bulk glass).

2.5.3. Fourier Transform Infrared Spectroscopy (FT-IR). The glass structural properties and the formation of an apatite-like phase on the scaffold surface were investigated by FT-IR (Impact 420 Nicolet, Thermo Scientific). For that, the glass or ground scaffolds were pressed into potassium bromide (KBr) pellets. The pellets were made by mixing 1 mg of sample and 300 mg of KBr (spectroscopy grade, Merck). Spectra were recorded between 2000 and 400 cm^{-1} with a resolution of 4 cm^{-1}. To compare the intensities of single bands, all spectra were normalized to the silica band at ∼1040 cm^{-1}.

2.5.4. Raman Spectroscopy. Raman spectra (LabRAM HR-Evolution, Horiba Scientific) of the glass powders were obtained using a diode-pumped solid state laser (YAG; λ = 532 nm). The hole, slit, and grating were set to 1000 μm, 100 μm, and 600 grooves/mm, respectively. The data acquisition time was 5 s, and averaging was performed over 20 measurements. The spectra were normalized to the intensity of the band centered at 630 cm^{-1}.

2.5.5. Inductively Coupled Plasma-Optical Emission Analyses (ICP-OES). Ion release of Co and Si species under quasi-dynamic conditions from scaffolds soaked in SBF was measured using the ICP-OES Optima 8300 instrument (Perkin Elmer). Seven-point calibrations (100, 50, 25, 10, 2.5, 1, and 0.1 ppm) were performed by diluting certified standards (Carl Roth) with SBF. For elemental analysis of the scaffolds after SBF soaking, the scaffolds (total mass of 20−50 mg) were digested in a microwave oven (Multiwave 3000, Anton Paar). The digestion solution comprised 2 mL of hydrofluoric acid (48%, supra purity, Roth Chemicals), 2 mL of nitric acid (69%, supra purity, Roth Chemicals), and 4 mL of hydrochloric acid (35%, supra purity, Roth Chemicals). After the microwave procedure, 2 g of boric acid (>99.8%, Roth Chemicals) was added and the total volume was set to 250 mL. A five-point calibration (50, 25, 10, 1, and 0.1 ppm) was performed by diluting certified elemental standards (Roth Chemicals) with the digestion solution. Errors given for all ICP-OES analyses are standard deviations of three independent soaking experiments.

2.5.6. X-ray Diffraction (XRD). X-ray diffraction analysis was performed using a D8 ADVANCE X-ray diffractometer (Bruker) in a 2θ range of 20−80° with Cu Kα radiation. BG-derived scaffolds were powdered and dispersed in ethanol. The solution was dripped on off-axis-cut, low-background silicon wafers (Bruker AXS). A step size of 0.014° with 1 s per step was used.

2.5.7. Micro-PIXE-RBS Analysis. Analyses of the glass scaffold−biological fluid interface were conducted using nuclear microprobes at CENBG (Centre d'Études Nucléaires de Bordeaux-Gradignan, Gradignan, France).[27] PIXE-RBS analyses were performed on the nanobeamline. We chose a proton scanning microbeam with a 3 MeV energy and a 60 pA intensity. The beam diameter was nearly 1 μm. An 80 mm^2 Si(Li) detector was used for X-ray detection, oriented at 135° with respect to the incident beam axis and equipped with a 12 μm thick beryllium window. An aluminum funny filter with a thickness of 100 μm with a hole 2 mm in diameter was added to the detector. SUPAVISIO was used to define the different regions of interest with the use of masks. These masks isolate the spectra corresponding to the region of interest for the calculation of the elemental composition in that region. Quantification of PIXE spectra was conducted using GUPIX[28] and is calibrated against NIST standard reference glass materials. This method allows a chemical analysis with an excellent sensitivity of several parts per million because of the very good signal to background ratio. Compared to other techniques like SEM−EDS, the PIXE method allows an improvement in the sensitivity of up to 3 orders of magnitude. This is a great advantage for studying the distribution and role of relevant bone trace elements used to dope scaffolds (Co) that can induce specific cellular responses or can modify the bioactive process. In relation to RBS, a silicon particle detector placed 135° from the incident beam axis provided us with the number of protons that interacted with the sample. Data were treated with the SIMNRA code.

To assess the *in vitro* bioactivity by ion beam measurements, after 1, 3, and 7 days the samples were gently washed with deionized water, dehydrated with acetone, and dried at 60 °C for 12 h. Then, the glass scaffolds were embedded in resin (AGAR). Before being characterized, the glass scaffolds were cut into thin sections with a nominal thickness of 500 μm using a low-speed diamond saw. Then, the sections were placed on a mylar film with a 3 mm hole in the center. This preparation protocol allowed us to obtain smooth sections that were needed to perform micro-ion beam analysis and allowed us to examine in detail the pore surface of the glass scaffolds.

2.5.8. Differential Scanning Calorimetry (DSC). Differential scanning calorimetry (DSC, 404 F1 Pegasus, Netzsch, Selb, Germany) was performed in an air atmosphere with a heating rate of 2 K/min, employing ∼25 mg of powder in Pt crucibles to determine the thermal behavior of the glasses, in terms of glass transition and crystallization.

3. RESULTS AND DISCUSSION

3.1. Glass Properties. Figure 1a shows the FT-IR spectra of Co-containing glasses in the as-fabricated state. The main

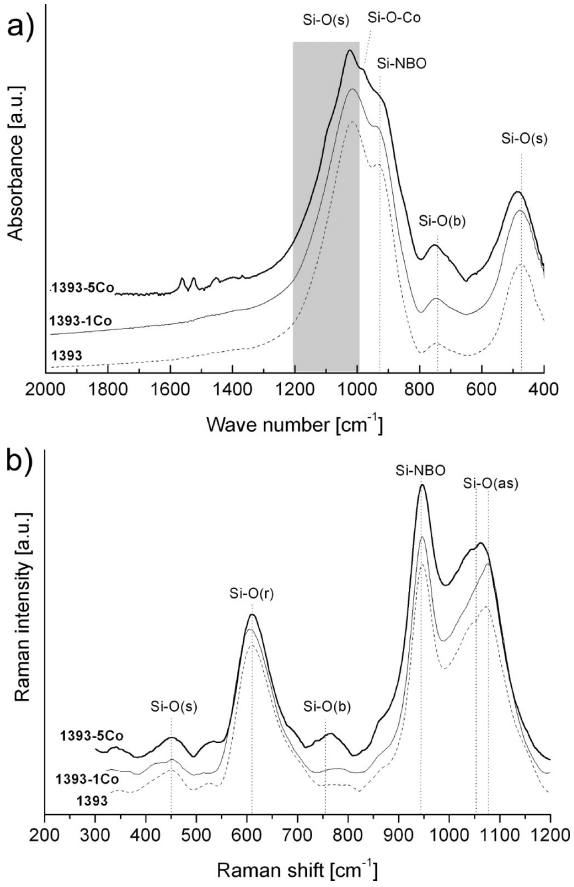

Figure 1. FT-IR (a) and Raman spectra (b) of Co-containing 1393 glass powder as fabricated.

absorption bands appearing in the spectra are summarized in Table 2. It can be observed that the intense band attributed to asymmetric stretching vibrations of the Si−O bond becomes sharper with an increasing Co content in the glass. Also, for 1393-5Co, an additional peak at ∼1105 cm^{-1} and a weak shoulder at ∼1205 cm^{-1} were detected, these are typically observed for silicate glasses with higher SiO_2 content and vitreous silica, respectively. The Si−NBO (nonbridging oxygen) peak (at ∼950 cm^{-1})[29] seems to have a reduced intensity and is slightly shifted to lower wavenumbers. In addition, the intensity of the bending mode of the Si−O band at ∼790 cm^{-1} increases with a higher Co content in the glass. Also, for 1393-

Table 2. Main Bands Appearing in the FT-IR and Raman Spectra of 1393-Co Glass Powders As Fabricated

assignment	FT-IR (cm^{-1})	Raman (cm^{-1})	remarks
symmetric stretching ν_{sym}(Si−O−Si)	∼490−500	∼450	ν_{sym}(Si−O−Si) at ∼450 cm^{-1} is observed for pure silica.[31] For bioactive glasses, the band is shifted to 500 cm^{-1}.[29] In the Raman spectra, this band is assigned to silica ring structures.[32]
asymmetric stretching ν_{asym}(Si−O−Si)	range from 1000 to 1300	∼1060−1080[33]	In the FT-IR spectra, the most intense Si−O band is found at ∼1040 cm^{-1}. Upon incorporation of Co into the glass structure, additional bands at ∼1140 and ∼1220 cm^{-1} are observed. Please note that these additional bands are typically seen in vitreous silica.
	∼1040/1140 − TO_1[a]		
	∼1220 − TO_2[a]		In the Raman spectra,[33] the peak maximum is shifted toward lower frequencies for 1393-5Co and 1393-10Co glasses.
bending mode δ(Si−O−Si)	peak at ∼750[29]	broad band at ∼750[33]	The intensity increases with the higher Co content in the glass.
rocking vibrations of Si−O−Si	not available	∼620[33]	–
SiO_{NBO}	shoulder at ∼930	peak at ∼940	In the FT-IR spectra, the intensity of the SiO_{NBO} is decreasing and SiO_{NBO} is shifted to lower frequencies upon incorporation of 5 and 10 wt % Co.[29,31]
Si−O−Co	992		Appears in the FT-IR spectra of 1393-5Co and 1393-10Co glass and is attributed to Si−O−Co bonding.[30]

[a]TO denotes transverse optical groups of Si−O−Si bonds.

5Co, an additional absorption peak was observed at ∼990 cm^{-1}, which according to the literature might be attributed to Si−O−Co bonds as it was shown for metal-containing mesoporous alumino-silicates (zeolites).[30] Hence, the FT-IR analysis gives an indication that for concentrations of ≥5 wt % Co is entering the glass network by forming Si−O−Co bonds, which might result in a more polymerized SiO_2 network.

Raman spectra of the 1393-Co glasses are depicted in Figure 1b. According to the literature, the wide absorption band at ∼1100 cm^{-1} can be assigned to the asymmetric stretching mode of the Si−O−Si group, whereas the bands at ∼610 and ∼930 cm^{-1} can be attributed to Si−O−Si rocking vibrations and the Si−NBO bond, respectively.[33,34] The band at ∼450 cm^{-1} is most likely assigned to defect lines of vitreous silica that are typically observed for silica ring structures.[32] The broad peak evolving at 750 cm^{-1} is assigned to the bending mode of Si−O−Si.[33] This band appears on the 1393-5Co and 1393-10Co spectra, which is likely due to the greater length of the Co−O bond (192 pm) compared with that of the Si−O bond (177 pm).

Figure 2 shows the DSC diagrams for the 1393-Co glass powders. The glass transition point (T_g) and the crystallization

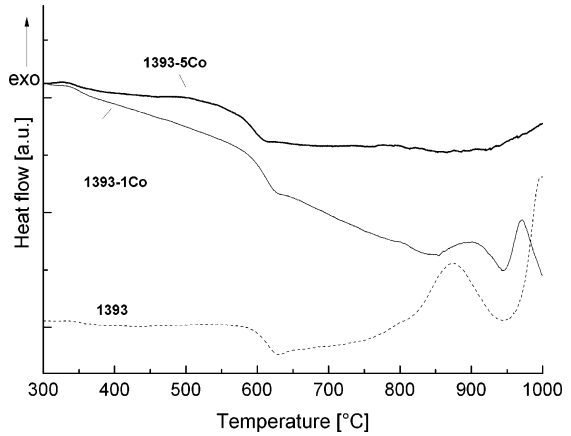

Figure 2. DSC analysis of powdered Co-containing 1393 glass compositions.

onset (T_c) derived from the DSC measurement are summarized in Table 3. T_g decreases continuously with an

Table 3. Characteristic Temperatures (°C) of the Co-Containing Glasses Derived from DSC Measurements

glass	1393	1393-1Co	1393-5Co	1393-10Co
T_g	626	621	606	587
$T_{c,onset}$	750	848	–[a]	–[a]

[a]Outside of the observed temperature range.

increasing Co^{2+} content in the glass, whereas $T_{c,onset}$ increases with a higher Co content. The process window for the glass fabrication is larger for the Co-containing glass, whereas Co stabilizes the amorphous glass state.

The effect of Co incorporation into the glass structure and its properties can be discussed on the basis of FT-IR as well as Raman spectroscopy and correlated with the glass thermal behavior as derived from DSC measurements. CoO is known to be an intermediate oxide and, thus, can enter the silicate network or act as a modifying oxide.[18] As the T_g decreased with incorporation of Co, it is likely that Co is entering the glass

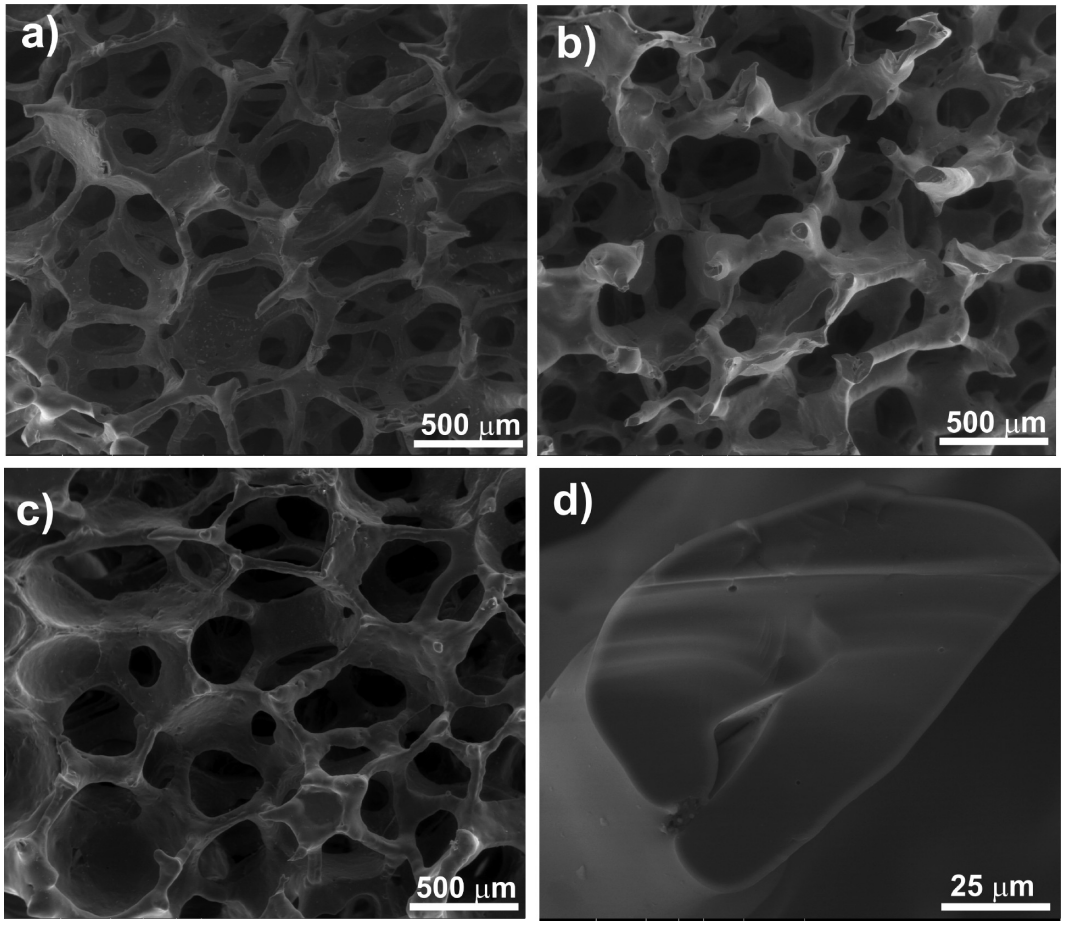

Figure 3. SEM images of the scaffold macrostructure for (a) 1393, (b) 1393-1Co, and (c) 1393-5Co glass compositions. (d) Higher-magnification image of a strut of a 1393-derived scaffold showing the dense structure and smooth surface.

network creating Si−O−Co bonds replacing the stronger Si−O−Si bonds.[18] Thus, the glass network becomes weaker, and T_g decreases.[18] This observation is in agreement with FT-IR results that indicated the formation of additional Si−O−Co bonds in the glass network as a result of Co substitution. However, according to FT-IR analysis (Figure 1a), the formation of Si−O−Co bonds is evident only for Co contents of 5 wt %. Hence, we conclude that Co plays a concentration-dependent role in the glass network, acting as network modifier at 1 wt % and a network former at ≥5 wt %. This corresponds to literature reports that also showed the concentration-dependent behavior of CoO in silicate glasses.[18] A lower T_g is associated with weaker bonds within the glass network and should therefore result in enhanced *in vitro* degradation of the glass scaffolds, which will be discussed in section 3.3.

3.2. Scaffold Properties. Scaffolds were prepared using the 1393, 1393-1Co, and 1393-5Co glasses.

XRD analysis of the scaffolds revealed that the scaffolds remain in the amorphous state; no crystalline phases were detected (data not shown). This is in agreement with DSC results shown above that revealed a crystallization onset temperature ($T_{c,onset}$) of >750 °C being above the sintering temperature, thus precluding crystallization during the densification process.

The macrostructure of the scaffolds derived from Co containing 1393 glasses is shown in Figure 3. No major differences between the glass compositions were observed. All scaffolds show completely interconnected pore systems with pore diameters of ∼200−400 μm. Single coated scaffolds showed porosities of 94, 93, and 95% for 1393, 1393-1Co, and 1393-5Co samples, respectively, confirming that the main macrostructural features are independent of the glass composition. For doubly coated scaffolds, slightly lower porosities of 91, 90, and 89% were found for 1393, 1393-1Co, and 1393-5Co, respectively.

High porosities and the interconnected pore system of the scaffold should allow vascularization and tissue ingrowth when the scaffold is applied as an engineered bone construct. Vascularization has been shown to be enhanced in scaffolds with >250 μm pores,[35] and high interconnectivity is thought to be an even more important factor for blood vessel and tissue ingrowth.[36,37] Thus, the 1393-Co-derived scaffolds meet the macrostructural requirements for use as bone tissue engineering scaffolds. In Figure 3d, a 1393 scaffold strut at a higher magnification is shown, revealing dense struts and a smooth scaffold surface without cracks. This is in agreement with literature reports that showed that 1393 bioactive glass can be densified by viscous flow sintering, preventing crystallization.[38]

Figure 4a shows typical stress−strain curves observed for doubly coated 1393-Co-derived scaffolds in compressive mode. We observed a catastrophic failure of the scaffolds at a given maximal stress (marked with asterisks in Figure 4a) followed by a rapid decrease in stress. The further increase in stress is correlated with the compression of the remaining scaffolds struts.[25]

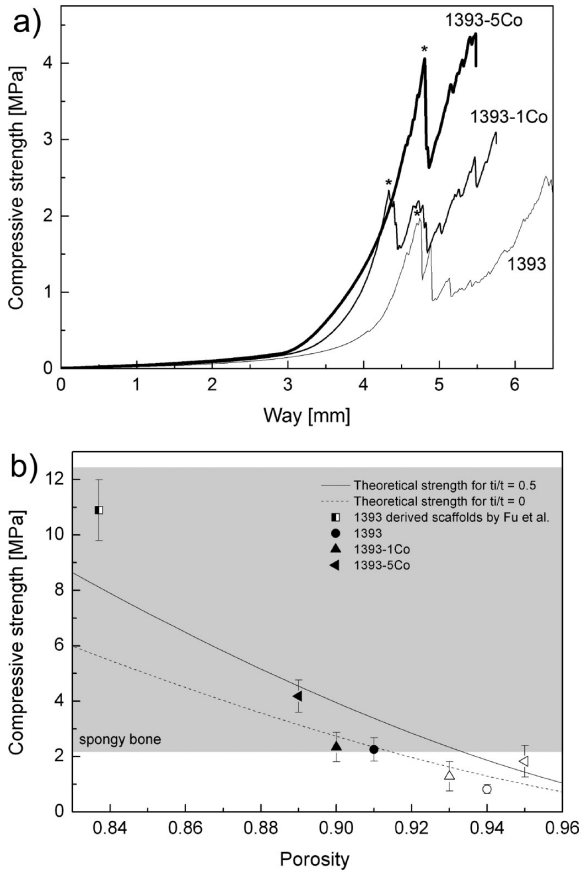

Figure 4. (a) Selected stress-way curves for a Co-containing 1393 scaffold series measured in compressive mode. Asterisks mark the scaffold failure. (b) Compressive strength mean values for 10 samples measured per scaffold series. Empty and full symbols represent single and double coated scaffolds, respectively.

Compressive strengths of 2.3 ± 0.4, 2.3 ± 0.5, and 4.2 ± 0.6 MPa for 1393, 1393-1Co, and 1393-5Co glass-derived scaffolds, respectively, were measured. However, to be able to compare the strengths among different glass compositions, the porosity of the scaffolds has to be taken into account. The theoretical strength (σ_{theo}) of cellular materials with open cells can be estimated by applying the model by Gibson and Ashby:[39]

$$\frac{\sigma_{theo}}{\sigma_{fs}} = C\left(\frac{\rho_{foam}}{\rho_{solid}}\right)^{3/2} \times \frac{1 + (t_i/t)^2}{\sqrt{1 - (t_i/t)^2}} \quad (1)$$

$$\frac{\sigma_{theo}}{\sigma_{fs}} = C(1 - P)^{3/2} \times \frac{1 + (t_i/t)^2}{\sqrt{1 - (t_i/t)^2}} \quad (2)$$

where σ_{fs} is the modulus of rupture of the cell wall material, C is a constant of proportionality (for brittle ceramics, C = 0.2), ρ_{foam} is the density of the foam, ρ_{solid} is the density of the solid ceramic, P is the porosity of the foam, and t_i/t is the ratio of the central void size of the strut to the strut diameter.

The modulus of rupture of a strut is defined as the maximal stress at failure. Given an average strut thickness of ∼100 μm, the tensile strength of 1393 fibers of 440 MPa (diameter of 93−160 μm) was taken to be σ_{fs}.[40] According to Figure 3d, the t_i/t ratio was estimated to be between 0 and 0.5. The theoretical strength and experimental values observed in this work are given in Figure 4b. Also, compressive strengths reported in literature for 1393 glass-derived scaffolds made by the foam replica technique are given for comparison.[38] The experimental data observed in our study follow the curve for the compressive strength as predicted by eq 2. Also noticeable is the fact that with a change in the foam replica regime the compressive strength of the scaffolds can be enhanced while a high porosity of 89−91% is maintained. Considering the differences in porosity, the compressive strengths of these scaffolds are comparable with values reported by Fu et al.[38] for 1393-derived scaffolds even though those values are greater than the theoretical strength (Figure 4b). The reason for this could be that for the theoretical calculation of the strength a constant modulus of rupture is assumed; in praxis, however, the rupture modulus is not a constant but varies following the Weibull distribution.[39] Also, the strengths reported for dense 1393 material (which is taken for calculations of the porous foams) contain a large deviation (440 ± 120 MPa), which allows only a rough estimation.

Overall, the σ_c values of the 1393-Co-derived scaffolds fabricated in this work correspond to the lower limits of human spongy bone, which allows the scaffolds to be used for regeneration of cancellous bone.[41]

3.3. *In Vitro* Degradation and Co Release in SBF.

3.3.1. HAp Formation. First, the reaction stages occurring on the surface of the scaffolds during reaction in SBF are shown to be exemplary for the plain 1393 scaffolds and are discussed on the basis of SEM, FT-IR, and PIXE-RBS analysis. In addition, the effect of incorporation of Co into the glass on the hydroxyapatite forming ability and degradation of the glass scaffolds is presented and discussed. Figure 5 shows the SEM analysis of 1393-derived scaffolds after immersion in SBF for 1 day (a and b), 3 days (c and d), and 7 days (e and f). After 1 day, the first indications of a surface reaction can be observed on the scaffold surface: a thin reaction layer has formed. However, the inner glass matrix remained intact without any signs of dissolution. After immersion for 3 days, three distinct areas and/or phases can be distinguished as indicated in Figure 5d: light gray area showing the inner BG network, a dark gray layer (SiO_2), and a thin layer on top (CaP). This distinction was made on the basis of the EDS analysis, as shown in Table 4. The thickness of these layers was roughly estimated from the SEM images to be 0.5−3 μm.

The SiO_2 reaction region is quite inhomogeneous, and hence, the estimated thicknesses are given with a large standard deviation. In fact, SEM analysis provides only rough estimations; more reliable data for the dimensions of the reaction layers are provided by PIXE-RBS analysis below. After further growth of the CaP layer for 7 days, the formation of the typical morphology of hydroxyapatite was observed. However, again, no clearly visible dissolution of the inner region of the scaffold strut was observed via SEM (Figure 5f).

3.3.2. Micro-PIXE-RBS-Derived Chemical Maps. To identify the origin of the phases formed on the BG scaffolds, quantitative chemical maps were determined by ion beam measurements; these give a more precise picture of the reactions taking place at the scaffold−fluid interface compared to the observation made by SEM−EDS. Ion beam analysis has been shown to be a powerful technique for identifying the reactions on the bioactive glass−fluid interface.[42]

In the as-fabricated state, Ca, Mg, P, and Si (Na and K are not shown for the sake of simplicity) are homogeneously distributed (see the Supporting Information).

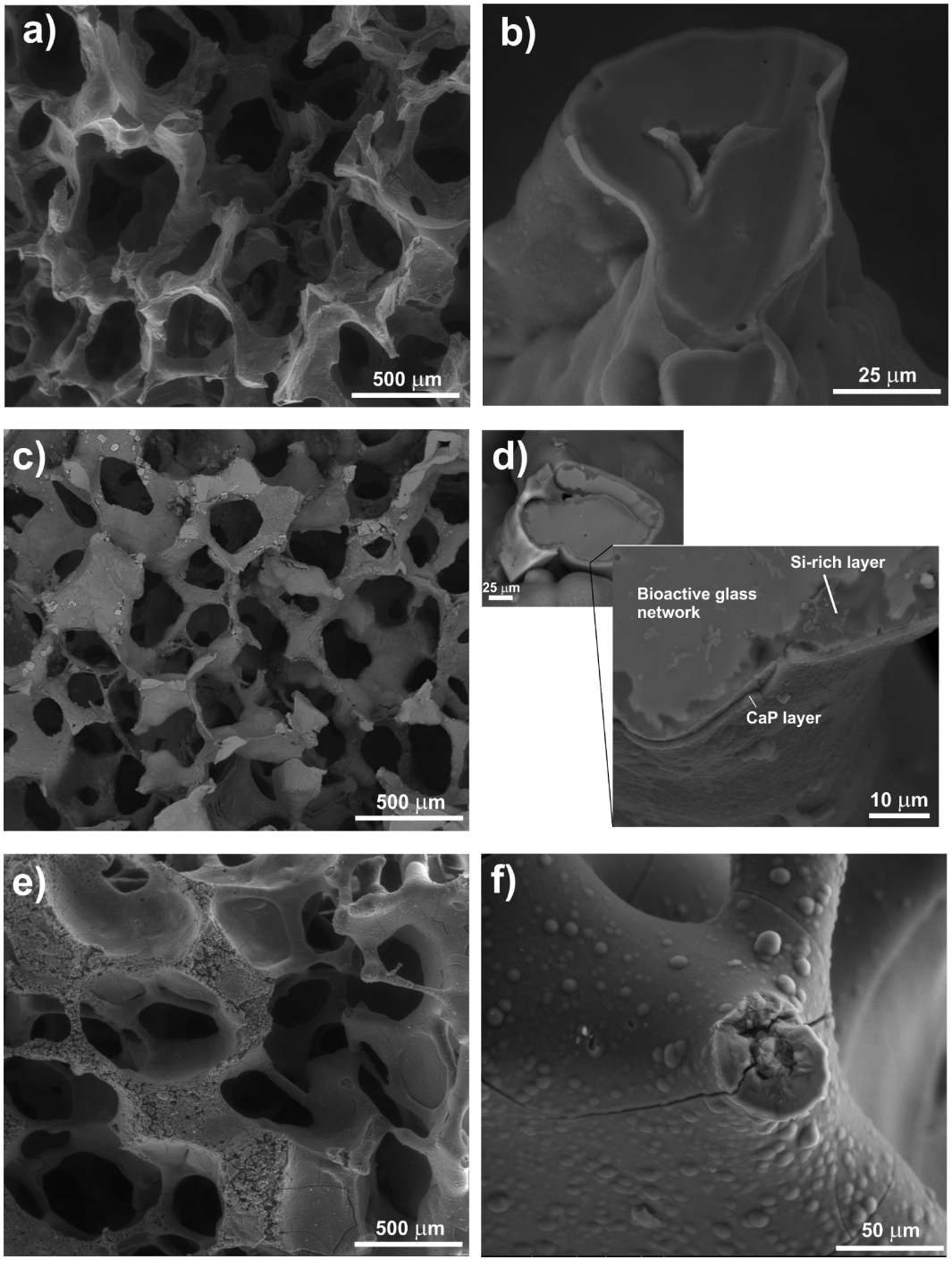

Figure 5. SEM analysis of 1393-derived scaffolds after immersion in SBF for 1 day (a and b), 3 days (c and d), and 7 days (e and f).

Table 4. EDS-Derived Elemental Concentrations (atom %) of the Reaction Phases Formed on 1393 Scaffolds after 3 Days in SBF

	Mg	K	Si	P	Ca	Ca/P
BG	2.79	4.74	20.30	1.34	6.71	5.00
SiO_2	0.63	1.23	26.21	1.32	2.02	1.53
CaP	1.21	0.93	14.87	4.87	6.80	1.40

Figure 6 shows PIXE-RBS-derived elemental maps for 1393 scaffolds after 1, 3, and 7 days. These results can be directly correlated to the SEM observations shown in Figure 5. Basically, according to the elemental maps, again three distinct regions during reaction in SBF can be defined: (i) inner region of the glass scaffolds (BG), (ii) silica-rich layer (SiO_2), and (iii) surface periphery (CaP layer).

Additionally, for regions of interest i and iii, the inner regions of the glass scaffolds and the scaffold periphery, respectively, the quantitative elemental concentrations were derived; they can be found in the Supporting Information. Interestingly, the inner part of the scaffolds did not show any signs of degradation: the elemental concentration in the inner region of the scaffolds remained constant for immersion times of up to 7 days for all glasses investigated. Hence, it is likely that the

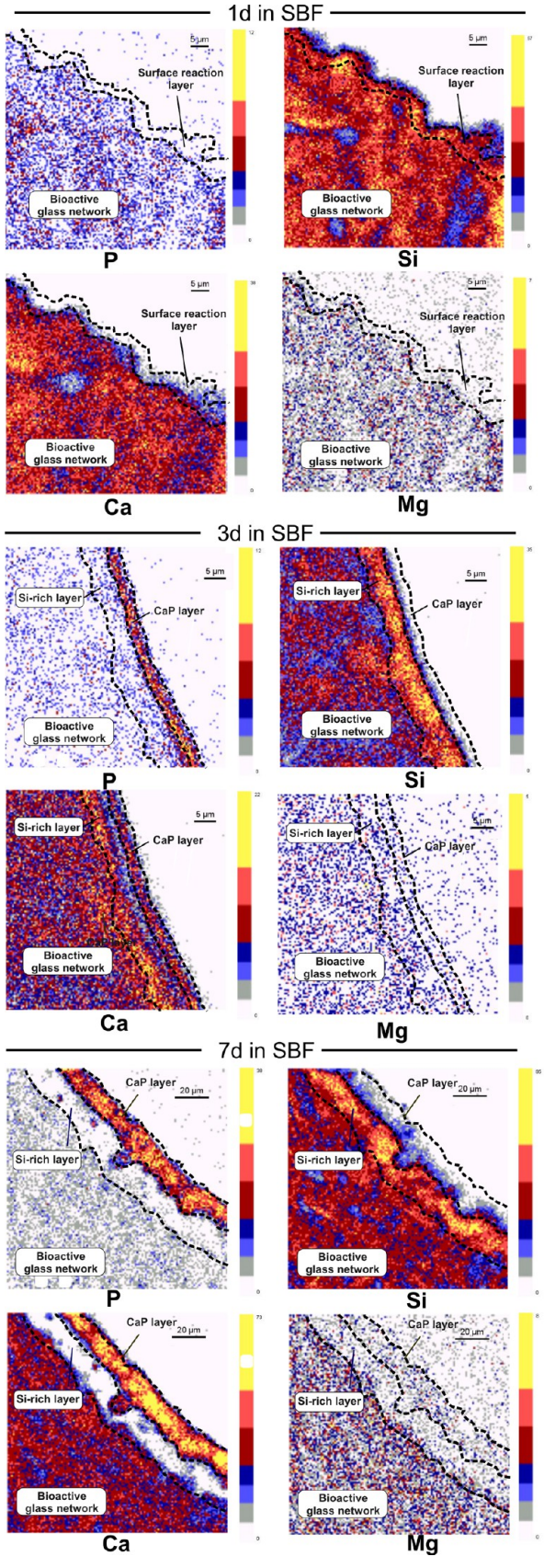

Figure 6. Elemental distribution in the cross section of a 1393 scaffold after reaction in SBF for 1, 3, and 7 days.

degradation of 1393-derived scaffolds occurs preferably at the scaffold interface with separate reaction stages as discussed below.

After immersion in SBF for 1 day, the first evidence of the initial surface reaction was observed: a thin (2.5 ± 0.4 μm) reaction layer was formed on the pore surface (Figure 6), which was depleted of Ca, P, and Mg, indicating fast release of these elements from the scaffold surface.

After 3 days (Figure 6), a silica-rich layer with a thickness of roughly 5.9 ± 0.5 μm was formed on the scaffold surface. This value is slightly larger than the value of 2.4 ± 1.7 μm observed via SEM (Figure 5). Considering the large deviation of the surface thickness as observed via SEM, we concluded that a SiO_2 layer with a thickness ranging between 1 and 6 μm is formed on the 1393-derived scaffold after reaction in SBF for 3 days. On top of it, a Ca- and P-enriched layer (3.1 ± 0.2 μm) was detected as already indicated by SEM–EDS analysis. This layer resulted from diffusion of Ca and P species from the glass network. As seen in the chemical maps, this Si-rich layer may be acting as a diffusion barrier given that Ca accumulated in the region right underneath the silica layer.

After 7 days, the glass surface was further dissolving; the Si-rich layer grew to a thickness of 18.0 ± 1.7 μm. Also, the CaP layer continued to grow, reaching 16.0 ± 0.2 μm. It is worth noting that traces of Mg were incorporated into the CaP layer, which is typical for biomimetic hydroxyapatite formed upon reaction in body fluids.[43,44] The thickness of the CaP layer was comparable to the results from our previous work conducted on 45S5 BG-derived scaffolds (~10 μm).[12]

Salinas et al.[45] observed the formation of a very thin CaP layer of ~2–3 μm on silicate scaffolds. However, this was measured on sol–gel-derived bioactive glasses[45,46] that are not directly comparable with the melt-derived 1393 glass investigated here. In fact, to the best of our knowledge, no data on the thickness of the hydroxyapatite layer formed on 1393-derived scaffolds upon immersion in SBF have been presented.

The effect of Co on the bioactivity of the 1393-1Co and 1393-5Co scaffolds is shown in Figures 7 and 8, respectively. In contrast to the reference 1393 glass scaffold, it is noticeable from the chemical maps that for 1393-1Co samples no distinct CaP layer is formed after 7 days in SBF (Figure 7). Even though P enrichment of the surface is clearly detectable, a rather mixed Si-rich CaP layer with traces of incorporated Co is observed.

For 1393-5Co scaffolds, however, a clearly distinguishable CaP layer was formed on top of the SiO_2 layer. Interestingly, Co is incorporated into the CaP layer. Co ions appear to diffuse through the SiO_2 layer (which itself is depleted of Co) and are substituted in the CaP layer.

One can speculate that the change in the chemistry of the CaP layer will have an impact on the cellular response. For instance, Co incorporated in calcium phosphates has been shown to increase the extent of osteoclast proliferation and overall mineral resorption.[47] To prove the formation of carbonate hydroxyapatite, FT-IR analysis was performed for the 1393-5Co scaffolds after 7 days in SBF as depicted in Figure 8 (bottom right panel). The formation of a crystalline carbonated hydroxyapatite can be monitored by the appearance of the triply generated (ν_3) bending modes of the O–P–O bands of CHA at 554 and 602 cm^{-1} as detected for 1393 and 1393-1Co scaffolds.[48] However, for the 1393-5Co sample, a broad band at ~600 cm^{-1} was observed, which is typical for

dx.doi.org/10.1021/am405354y | ACS Appl. Mater. Interfaces 2014, 6, 2865–2877

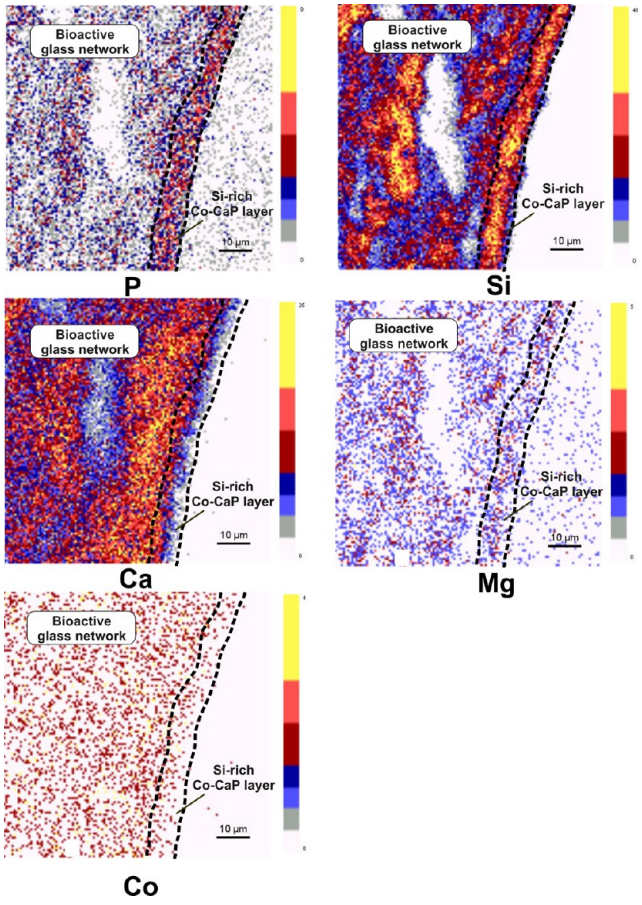

Figure 7. Elemental distribution in the cross section of a 1393-1Co scaffold after 7 days.

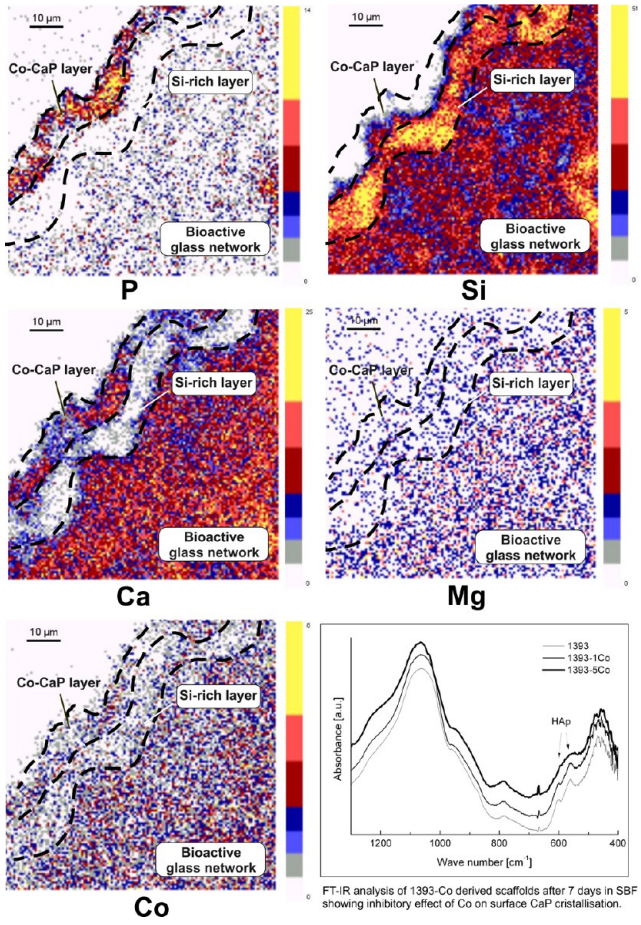

Figure 8. Elemental distribution in the cross section of a 1393-5Co scaffold after 7 days. The bottom right panel shows the FT-IR spectra of 1393-Co-derived scaffolds after immersion in SBF for 7 days.

amorphous CaP.[49] This is most likely due to large amounts of Co incorporated into the CaP layer (5 wt % as calculated from micro-PIXE-RBS analyses as shown in the Supporting Information). Basically, the kinetics of CaP layer formation among the 1393-Co glasses investigated are similar. However, the nature of this layer seems to differ: for 1393, a clearly distinguishable CaP layer with characteristics of carbonated hydroxyapatite was found, whereas for 1393-1Co, a rather mixed Ca−P−Si enriched layer was detected. Both were confirmed by FT-IR analysis to be carbonated hydroxyapatite, while the CaP layer formed on the 1393-5Co scaffolds is amorphous.

Our results obtained from SEM−EDS and micro-PIXE-RBS analyses confirm the well-known mechanism of the BG surface reaction and transformation to a calcium phosphate phase, including the formation of silanol groups and the condensation of a silica layer followed by the formation of an amorphous calcium phosphate (ACP) layer and its crystallization to carbonated hydroxyapatite (CHA).[12,51,52] However, in our study, an overly high Co content (and release) leads to inhibition of the ACP layer crystallization remaining in its amorphous state. It has been shown that addition of Co in the hydroxyapatite (HAp) lattice has an influence on the phase stability of HAp, leading to co-formation of brushite.[50]

3.3.3. Degradation and Ion Release in SBF. Cumulative ion concentrations of Si and Co released from the 1393-Co-derived scaffolds are shown in Figure 9. The overall degradation of the scaffolds can be tracked with Si release being the main marker of the glass network dissolution. Two different regions can be distinguished in the Si release profile of the 1393 scaffolds: (i) initial burst release of Si levels during the first days of the reaction and (ii) plateau of Si levels. Accordingly, the absolute values of the ion concentration for each time point (data not shown) describe the kinetics of Si release: for 1393 glass, an initial peak of Si release is reached after 3 days with maximal Si levels of 10 ppm and a further decrease in absolute Si levels to 0−1 ppm.

Maximal cumulative Si levels of 30 ppm were detected for the 1393 scaffolds after immersion for 21 days. In the literature, Si values of ∼60 ppm released from 45S5 particulate glass were reported by Cerruti et al.,[29] which is due to the reactivity of 45S5 glass being higher than that of 1393 glass and other glass compositions with higher SiO_2 contents. Even higher Si levels were shown by Jones et al.,[53] who reported 100−120 ppm Si released from sol−gel-derived 3D scaffolds.

The decrease in the Si release rates corresponds to the formation of a CaP layer that seems to be acting as a diffusion barrier leading to a decreased level of Si release. Similarly, for the 1393-5Co scaffolds, peaking Si values were observed after 3 days. However, the Si concentration of 18 ppm was significantly higher than that of the 1393 glass, which can be explained by the weaker glass structure caused through Co substitution as derived from DSC measurements (lower T_g). For the 1393-1Co samples, in turn, the Si peak is delayed, occurring after immersion in SBF for 14 days. This is in agreement with PIXE-RBS results that showed that in contrast to 1393 and 1393-5Co

dx.doi.org/10.1021/am405354y | ACS Appl. Mater. Interfaces 2014, 6, 2865−2877

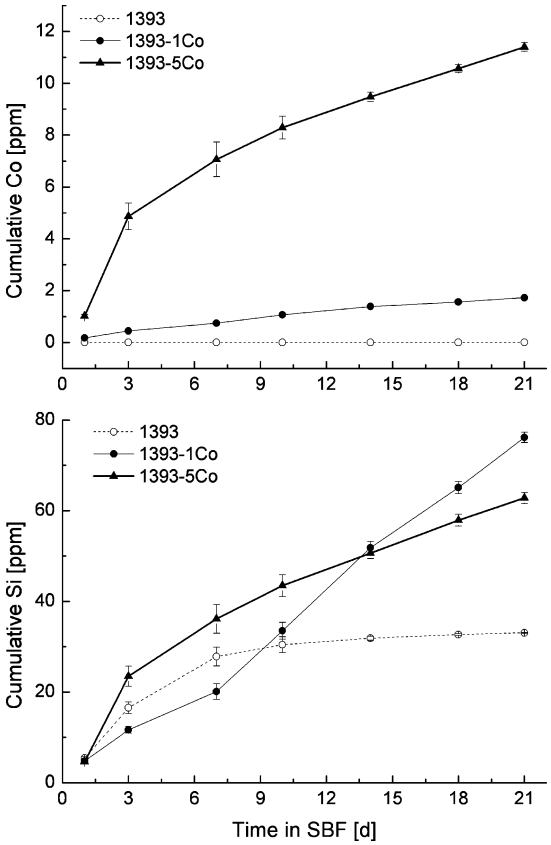

Figure 9. Release of accumulated Co and Si from Co-containing BG scaffolds in SBF.

scaffolds for the 1393-1Co series no distinct CaP layer was formed until the longest time period investigated had passed (7 days in SBF). Hence, the passivating CaP layer is likely to form at a later stage, thus retarding the release of Si from the 1393-1Co samples.

Co is continuously released from the scaffolds, reaching maximal cumulative values of 2 and 12 ppm for 1393-1Co and 1393-5Co samples, respectively. With regard to the absolute values released after each time point of measurement, the highest Co release rate occurs in the first 3 days of immersion (data not shown). It is most evident for the 1393-5Co samples showing a Co peak of ∼4 ppm after immersion in SBF for 3 days. For longer immersion times, the Co levels decrease to 1 ppm after 7 days, remaining at this level during immersion for a further 21 days. This is likely due to the formation of a CaP layer on the scaffold surface after 3 days as we observed from SEM and PIXE-RBS analysis. This layer could act as a diffusion barrier leading to a decrease in the rate of Co released into SBF.

After 21 days in SBF, the change in the scaffold mass was 4.3 ± 0.6, −18.7 ± 0.6, and −39.6 ± 0.6% for 1393, 1393-1Co, and 1393-5Co scaffolds, respectively. The increase in mass in the 1393 samples must be due to the formation of the calcium phosphate layer on the scaffold surface. At the same time, the 1393 scaffold showed the lowest degradation rates according to ICP measurements. After immersion in SBF for 7 days, the rate of Si release decreased to values close to 0 ppm, possibly because of the formation of a CaP layer acting as a diffusion barrier. In this way, the cumulative values of Si released in SBF quickly reached a plateau at ∼30 ppm. Hence, we conclude that the dissolution of 1393-derived scaffolds is almost completely impeded after reaction in SBF for 7 days. The weight gain measured for the 1393 scaffolds is contradictory to literature reports. For example, Fu et al.[54] observed a weight loss of ∼5% for 1393 foam replica-derived scaffolds with porosity values similar to that of our scaffolds (85%). However, in contrast to our study, Fu et. renewed the SBF solution more frequently (every 24 h), which could have led to enhanced scaffold degradation due to the presence of a significant concentration gradient during the experiment resulting in a higher rate of scaffold degradation.

In contrast, for cobalt-containing scaffolds, a continuous release of Si was detected over a reaction time range of 21 days. Even though for these samples a decrease in absolute Si values released was also observed, the Si release rates remained high (∼1.5−3 ppm/day).

After the degradation study, the scaffolds were digested and the fractions of the remaining oxides were calculated. With regard to the SiO_2 content, the relative concentrations of the elements are listed in Table 5. The glass scaffold compositions after the degradation study reflect the dissolution behavior of the scaffolds as shown above. For Co-containing samples, a greater loss of Ca and P is observed compared to 1393 glass, which corresponds to higher Si release rates in SBF. Similarly, the loss of Na is greatest for 1393-5Co scaffolds. For Co-containing samples, residual amounts of CoO of 2 and 3 wt % were observed for 1393-1Co and 1393-5Co samples, respectively.

We have shown that the 1393 glass matrix is suitable for the controlled release of Co ions in a physiological environment. Similarly, Azevedo et al.[18] reported Co values of ∼13 ppm released from melt-derived glasses in Tris buffer after 21 days without refreshing the solution. Also, Wu et al.[23] showed that maximal Co levels of ∼20 ppm are released from Co-containing sol−gel-derived scaffolds in a controllable manner. Because overly high Co concentrations can be toxic, a controlled release mechanism is essential for applications of such Co-releasing constructs. Our results show that 1393 glass-derived scaffolds can be used for the controlled release of Co^{2+} ions with controlled release rates (after the initial burst release) of 0.3 and 0.1 ppm/day depending on the glass composition.

The Co concentrations we found in our study are comparable to the values reported to be in the therapeutically active range. It has been shown, for instance, that treatment with 50, 100, and 200 μM $CoCl_2$, corresponding to 12, 24, and 48 ppm, respectively, stimulated migration, proliferation, and tubule-like structure formation of umbilical cord blood-derived CD133(+) cells, hence indicating the angiogenic potential of Co inducing hypoxic conditions.[55] Another study confirmed

Table 5. Oxide Contents Normalized to Silica in the Glass Remaining after the Degradation Study

glass	CaO	P_2O_5	NaO	MgO	CoO
1393	0.45 ± 0.02	0.51 ± 0.06	0.14 ± 0.00	0.05 ± 0.02	–
1393-1Co	0.37 ± 0.03	0.44 ± 0.04	0.14 ± 0.02	0.04 ± 0.02	0.02 ± 0.01
1393-5Co	0.08 ± 0.02	0.08 ± 0.02	0.06 ± 0.01	0.02 ± 0.01	0.03 ± 0.01

that treating human microvascular endothelial cells (HMEC-1) with 12 ppm $CoCl_2$ also induced binding of HIF-1 and hence mediated transcriptional responses to hypoxia.[56] However, there has also been an indication that Co levels of >10 ppm might be cytotoxic as treatment of osteoblast-like MG63 cells with 10 ppm Co^{2+} resulted in a 40% decrease in cell number.[57] Similarly, Wu et al.[23] observed that a Co^{2+} concentration of ~20 ppm reduced the viability of bone marrow-derived stem cells (BMSCs) even though the Co^{2+} did not cause significant cytotoxicity.

Hence, the release of ~2 ppm from 1393-1Co may be considered noncritical with regard to potential cytotoxicity, whereas 11 ppm released from 1393-5Co might be at the upper edge of the therapeutical, nontoxic range. Altogether, the addition of Co to the 1393 glass network results in the weakening of the glass structure, leading to faster dissolution of the glass. In this manner, the degradation of the scaffolds can be adjusted by tailoring the composition of the glass, hence allowing the controlled release of ionic species. We showed that CoO acts as network modifier and a network former depending on its concentration in the glass. That way, the 1393 glass matrix might be used as a carrier for the controlled release of other therapeutic ions like ZnO or MgO also known to act as intermediate oxides in silicate glasses.[58]

4. CONCLUSION

We fabricated Co-containing 1393 bioactive glass-derived scaffolds with relatively high compressive strength values of 2.3 ± 0.4, 2.3 ± 0.5, and 4.2 ± 0.6 MPa for 1393, 1393-1Co, and 1393-5Co glass-derived scaffolds, respectively. Further, acellular *in vitro* studies revealed the rapid transformation of the glass surface to a calcium phosphate layer after 7 days in biological fluid, which is an essential feature for use in bone tissue engineering. It was shown that 1393 bioactive glass-derived scaffolds can be used as platforms for controlled Co release, which is within therapeutic ranges and can be adjusted by tailoring the glass composition. Detailed quantitative chemical maps from the scaffold–fluid interface derived from advanced micro-PIXE-RBS analyses revealed that Co is incorporated into the surface calcium phosphate layer. Considering the impact of surface chemistry on cell attachment and proliferation, these new insights into the physicochemical reactions at the scaffold–fluid interface will be important for improving our understanding of the mineralization behavior and cell response to bioactive glass scaffolds. These novel Co-releasing 1393 BG-derived scaffolds might be thus used as hypoxia-mimicking biomaterials with a high degree of mechanical integrity, making them interesting candidates for bone tissue engineering applications.

■ ASSOCIATED CONTENT

Supporting Information

Chemical map of the cross section of reference 1393 scaffolds without SBF treatment and elemental evolution in the inner region and the periphery of Co-containing 1393 scaffolds as a function of immersion time in SBF. This material is available free of charge via the Internet at http://pubs.acs.org.

■ AUTHOR INFORMATION

Corresponding Author

*E-mail: aldo.boccaccini@ww.uni-erlangen.de.

Notes

The authors declare no competing financial interest.

■ ACKNOWLEDGMENTS

Florian Ruther is gratefully acknowledged for experimental support. Eva Springer (Institute of Glass and Ceramic, University of Erlangen-Nuremberg) is acknowledged for SEM analysis.

■ REFERENCES

(1) Hench, L. L. Bioceramics: From concept to clinic. *J. Am. Ceram. Soc.* **1991**, *74* (7), 1487–1510.
(2) Rahaman, M. N.; Day, D. E.; Bal, B. S.; Fu, Q.; Jung, S. B.; Bonewald, L. F.; Tomsia, A. P. Bioactive glass in tissue engineering. *Acta Biomater.* **2011**, *7* (6), 2355–2373.
(3) Hench, L. L. Genetic design of bioactive glass. *J. Eur. Ceram. Soc.* **2009**, *29* (7), 1257–1265.
(4) Jones, J. R. Review of bioactive glass: From Hench to hybrids. *Acta Biomater.* **2013**, *9* (1), 4457–4486.
(5) Santos, M. I.; Reis, R. L. Vascularization in bone tissue engineering: Physiology, current strategies, major hurdles and future challenges. *Macromol. Biosci.* **2010**, *10* (1), 12–27.
(6) Boccaccini, A. R.; Kneser, U.; Arkudas, A. Scaffolds for vascularized bone regeneration: Advances and challenges. *Expert Rev. Med. Devices* **2012**, *9* (5), 457–460.
(7) Hoppe, A.; Mourino, V.; Boccaccini, A. R. Therapeutic inorganic ions in bioactive glasses to enhance bone formation and beyond. *Biomater. Sci.* **2013**, *1* (3), 254–256.
(8) Habibovic, P.; Barralet, J. E. Bioinorganics and biomaterials: Bone repair. *Acta Biomater.* **2011**, *7* (8), 3013–3026.
(9) Hoppe, A.; Güldal, N. S.; Boccaccini, A. R. A review of the biological response to ionic dissolution products from bioactive glasses and glass-ceramics. *Biomaterials* **2011**, *32* (11), 2757–2774.
(10) Thompson, K. H.; Orvig, C. Boon and Bane of Metal Ions in Medicine. *Science* **2003**, *300* (5621), 936.
(11) Mouriño, V.; Cattalini, J. P.; Boccaccini, A. R. Metallic ions as therapeutic agents in tissue engineering scaffolds: An overview of their biological applications and strategies for new developments. *J. R. Soc., Interface* **2012**, *9* (68), 401–419.
(12) Hoppe, A.; Meszaros, R.; Stahli, C.; Romeis, S.; Schmidt, J.; Peukert, W.; Marelli, B.; Nazhat, S. N.; Wondraczek, L.; Lao, J.; Jallot, E.; Boccaccini, A. R. In vitro reactivity of Cu doped 45S5 Bioglass® derived scaffolds for bone tissue engineering. *J. Mater. Chem. B* **2013**, *1* (41), 5659–5674.
(13) Stähli, C.; Muja, N.; Nazhat, S. N. Controlled copper ion release from phosphate-based glasses improves human umbilical vein endothelial cell survival in a reduced nutrient environment. *Tissue Eng., Part A* **2013**, *19* (3-4), 548–557.
(14) Barralet, J.; Gbureck, U.; Habibovic, P.; Vorndran, E.; Gerard, C.; Doillon, C. J. Angiogenesis in calcium phosphate scaffolds by inorganic copper ion release. *Tissue Eng., Part A* **2009**, *15* (7), 1601–1609.
(15) Mourino, V.; Newby, P.; Boccaccini, A. R. Preparation and characterization of gallium releasing 3-D alginate coated 45S5 bioglass® based scaffolds for bone tissue engineering. *Adv. Eng. Mater.* **2010**, *12* (7), B283–B291.
(16) Wan, C.; Gilbert, S. R.; Wang, Y.; Cao, X.; Shen, X.; Ramaswamy, G.; Jacobsen, K. A.; Alaql, Z. S.; Eberhardt, A. W.; Gerstenfeld, L. C.; Einhorn, T. A.; Deng, L.; Clemens, T. L. Activation of the hypoxia-inducible factor-1α pathway accelerates bone regeneration. *Proc. Natl. Acad. Sci. U.S.A.* **2008**, *105* (2), 686–691.
(17) Emans, P. J.; Spaapen, F.; Surtel, D. A. M.; Reilly, K. M.; Cremers, A.; van Rhijn, L. W.; Bulstra, S. K.; Voncken, J. W.; Kuijer, R. A novel in vivo model to study endochondral bone formation; HIF-1α activation and BMP expression. *Bone* **2007**, *40* (2), 409–418.
(18) Azevedo, M. M.; Jell, G.; O'Donnell, M. D.; Law, R. V.; Hill, R. G.; Stevens, M. M. Synthesis and characterization of hypoxia-

mimicking bioactive glasses for skeletal regeneration. *J. Mater. Chem.* **2010**, *20* (40), 8854−8864.
(19) Peters, K.; Schmidt, H.; Unger, R.; Kamp, G.; Pröls, F.; Berger, B.; Kirkpatrick, C. J. Paradoxical effects of hypoxia-mimicking divalent cobalt ions in human endothelial cells in vitro. *Mol. Cell. Biochem.* **2005**, *270* (1-2), 157−166.
(20) Chachami, G.; Simos, G.; Hatziefthimiou, A.; Bonanou, S.; Molyvdas, P.-A.; Paraskeva, E. Cobalt Induces Hypoxia-Inducible Factor-1α Expression in Airway Smooth Muscle Cells by a Reactive Oxygen Species- and PI3K-Dependent Mechanism. *Am. J. Respir. Cell Mol. Biol.* **2004**, *31* (5), 544−551.
(21) Tanaka, T.; Kojima, I.; Ohse, T.; Ingelfinger, J. R.; Adler, S.; Fujita, T.; Nangaku, M. Cobalt promotes angiogenesis via hypoxia-inducible factor and protects tubulointerstitium in the remnant kidney model. *Lab. Invest.* **2005**, *85* (10), 1292−1307.
(22) Buttyan, R.; Chichester, P.; Stisser, B.; Matsumoto, S.; Ghafar, M. A.; Levin, R. M. Acute intravesical infusion of a cobalt solution stimulates a hypoxia response, growth and angiogenesis in the rat bladder. *J. Urol.* **2003**, *169* (6), 2402−2406.
(23) Wu, C.; Zhou, Y.; Fan, W.; Han, P.; Chang, J.; Yuen, J.; Zhang, M.; Xiao, Y. Hypoxia-mimicking mesoporous bioactive glass scaffolds with controllable cobalt ion release for bone tissue engineering. *Biomaterials* **2012**, *33* (7), 2076−2085.
(24) O'Donnell, M. D.; Hill, R. G. Influence of strontium and the importance of glass chemistry and structure when designing bioactive glasses for bone regeneration. *Acta Biomater.* **2010**, *6* (7), 2382−2385.
(25) Chen, Q. Z.; Thompson, I. D.; Boccaccini, A. R. 45S5 Bioglass®-derived glass-ceramic scaffolds for bone tissue engineering. *Biomaterials* **2006**, *27* (11), 2414−2425.
(26) Kokubo, T.; Takadama, H. How useful is SBF in predicting in vivo bone bioactivity? *Biomaterials* **2006**, *27* (15), 2907−2915.
(27) Incerti, S.; Zhang, Q.; Andersson, F.; Moretto, P.; Grime, G. W.; Merchant, M. J.; Nguyen, D. T.; Habchi, C.; Pouthier, T.; Seznec, H. Monte Carlo simulation of the CENBG microbeam and nanobeam lines with the Geant4 toolkit. *Nucl. Instrum. Methods Phys. Res., Sect. B* **2007**, *260* (1), 20−27.
(28) Maxwell, J. A.; Teesdale, W. J.; Campbell, J. L. The Guelph PIXE software package II. *Nucl. Instrum. Methods Phys. Res., Sect. B* **1995**, *95* (3), 407−421.
(29) Cerruti, M.; Greenspan, D.; Powers, K. Effect of pH and ionic strength on the reactivity of Bioglass® 45S5. *Biomaterials* **2005**, *26* (14), 1665−1674.
(30) Selvaraj, M.; Kim, B. H.; Lee, T. G. FTIR Studies on Selected Mesoporous Metallosilicate Molecular Sieves. *Chem. Lett.* **2005**, *34* (9), 1290−1291.
(31) Bunker, B. C.; Tallant, D. R.; Headley, T. J.; Turner, G. L.; Kirkpatrick, R. J. Structure of leached sodium borosilicate glass. *Phys. Chem. Glasses* **1988**, *29* (3), 106−120.
(32) Geissberger, A. E.; Galeener, F. L. Raman studies of vitreous SiO_{2} versus fictive temperature. *Phys. Rev. B: Solid State* **1983**, *28* (6), 3266−3271.
(33) González, P.; Serra, J.; Liste, S.; Chiussi, S.; León, B.; Pérez-Amor, M. Raman spectroscopic study of bioactive silica based glasses. *J. Non-Cryst. Solids* **2003**, *320* (1−3), 92−99.
(34) McMillan, P. F.; Wolf, G. H.; Poe, B. T. Vibrational spectroscopy of silicate liquids and glasses. *Chem. Geol.* **1992**, *96* (3−4), 351−366.
(35) Druecke, D.; Langer, S.; Lamme, E.; Pieper, J.; Ugarkovic, M.; Steinau, H. U.; Homann, H. H. Neovascularization of poly(ether ester) block-copolymer scaffolds in vivo: Long-term investigations using intravital fluorescent microscopy. *J. Biomed. Mater. Res., Part A* **2004**, *68* (1), 10−18.
(36) Karageorgiou, V.; Kaplan, D. Porosity of 3D biomaterial scaffolds and osteogenesis. *Biomaterials* **2005**, *26* (27), 5474−5491.
(37) Yang, S.; Leong, K. F.; Du, Z.; Chua, C. K. The design of scaffolds for use in tissue engineering. Part I. Traditional factors. *Tissue Eng.* **2001**, *7* (6), 679−689.
(38) Fu, Q.; Rahaman, M. N.; Bal, B. S.; Brown, R. F.; Day, D. E. Mechanical and in vitro performance of 13-93 bioactive glass scaffolds prepared by a polymer foam replication technique. *Acta Biomater.* **2008**, *4* (6), 1854−1864.
(39) Gibson, L. J.; Ashby, M. F. *Cellular solids: Structure and properties*; Cambridge University Press: Cambridge, U.K., 1999.
(40) Pirhonen, E.; Niiranen, H.; Niemelä, T.; Brink, M.; Törmälä, P. Manufacturing, mechanical characterization, and in vitro performance of bioactive glass 13-93 fibers. *J. Biomed. Mater. Res., Part B* **2006**, *77* (2), 227−233.
(41) Fu, Q.; Saiz, E.; Rahaman, M. N.; Tomsia, A. P. Bioactive glass scaffolds for bone tissue engineering: State of the art and future perspectives. *Mater. Sci. Eng., C* **2011**, *31* (7), 1245−1256.
(42) Jallot, E.; Lao, J.; John, Ł.; Soulié, J.; Moretto, P.; Nedelec, J. M. Imaging Physicochemical Reactions Occurring at the Pore Surface in Binary Bioactive Glass Foams by Micro Ion Beam Analysis. *ACS Appl. Mater. Interfaces* **2010**, *2* (6), 1737−1742.
(43) Lao, J.; Nedelec, J. M.; Jallot, E. New insight into the physicochemistry at the interface between sol-gel-derived bioactive glasses and biological medium: A PIXE-RBS study. *J. Phys. Chem. C* **2008**, *112* (25), 9418−9427.
(44) Müller, L.; Müller, F. A. Preparation of SBF with different content and its influence on the composition of biomimetic apatites. *Acta Biomater.* **2006**, *2* (2), 181−189.
(45) Salinas, A. J.; Vallet-Regi, M.; Izquierdo-Barba, I. Biomimetic Apatite Deposition on Calcium Silicate Gel Glasses. *J. Sol-Gel Sci. Technol.* **2001**, *21* (1-2), 13−25.
(46) Salinas, A. J.; Martin, A. I.; Vallet-Regí, M. Bioactivity of three $CaO-P_2O_5-SiO_2$ sol-gel glasses. *J. Biomed. Mater. Res.* **2002**, *61* (4), 524−532.
(47) Patntirapong, S.; Habibovic, P.; Hauschka, P. V. Effects of soluble cobalt and cobalt incorporated into calcium phosphate layers on osteoclast differentiation and activation. *Biomaterials* **2009**, *30* (4), 548−555.
(48) Koutsopoulos, S. Synthesis and characterization of hydroxyapatite crystals: A review study on the analytical methods. *J. Biomed. Mater. Res.* **2002**, *62* (4), 600−612.
(49) Layrolle, P.; Ito, A.; Tateishi, T. Sol-Gel Synthesis of Amorphous Calcium Phosphate and Sintering into Microporous Hydroxyapatite Bioceramics. *J. Am. Ceram. Soc.* **1998**, *81* (6), 1421−1428.
(50) Bose, S.; Fielding, G.; Tarafder, S.; Bandyopadhyay, A. Understanding of dopant-induced osteogenesis and angiogenesis in calcium phosphate ceramics. *Trends Biotechnol.* **2013**, *31* (10), 594−605.
(51) Hench, L. L. Bioceramics. *J. Am. Ceram. Soc.* **1998**, *81* (7), 1705−1728.
(52) Kokubo, T.; Kushitani, H.; Ohtsuki, C.; Sakka, S.; Yamamuro, T. Chemical reaction of bioactive glass and glass-ceramics with a simulated body fluid. *J. Mater. Sci.: Mater. Med.* **1992**, *3* (2), 79−83.
(53) Jones, J.; Ehrenfried, L.; Saravanapavan, P.; Hench, L. Controlling ion release from bioactive glass foam scaffolds with antibacterial properties. *J. Mater. Sci.: Mater. Med.* **2006**, *17* (11), 989−996.
(54) Fu, H.; Fu, Q.; Zhou, N.; Huang, W.; Rahaman, M. N.; Wang, D.; Liu, X. In vitro evaluation of borate-based bioactive glass scaffolds prepared by a polymer foam replication method. *Mater. Sci. Eng., C* **2009**, *29* (7), 2275−2281.
(55) Zan, T.; Du, Z. J.; Li, H.; Li, Q. F.; Gu, B. Cobalt chloride enhances angiogenic potential of CD133(+) cells. *Front. Biosci., Landmark Ed.* **2012**, *17*, 2247−2258.
(56) Minchenko, A.; Caro, J. Regulation of endothelin-1 gene expression in human microvascular endothelial cells by hypoxia and cobalt: Role of hypoxia responsive element. *Mol. Cell. Biochem.* **2000**, *208* (1−2), 53−62.
(57) Fleury, C.; Petit, A.; Mwale, F.; Antoniou, J.; Zukor, D. J.; Tabrizian, M.; Huk, O. L. Effect of cobalt and chromium ions on human MG-63 osteoblasts in vitro: Morphology, cytotoxicity, and oxidative stress. *Biomaterials* **2006**, *27* (18), 3351−3360.

(58) Watts, S. J.; Hill, R. G.; O'Donnell, M. D.; Law, R. V. Influence of magnesia on the structure and properties of bioactive glasses. *J. Non-Cryst. Solids* **2010**, *356* (9−10), 517−524.